Original Article
MOGS promotes stemness acquisition and invasion via enhancing NOTCH1-glycosylation dependent NOTCH pathway in colorectal cancer

Shihai Zhou[1*], Hongyun Huang[2*], Zheng Zheng[1], Kehong Zheng[3], Lang Xie[3]

[1]Department of Tumor Surgery, Zhongshan City People's Hospital, Zhongshan 528403, Guangdong, China; [2]Department of General Surgery, Peking Union Medical College Hospital, Chinese Academy of Medical Science and Peking Union Medical College, Beijing 100730, China; [3]Department of General Surgery, Zhujiang Hospital, Southern Medical University, Guangzhou 510280, Guangdong, China. *Equal contributors.

Abstract: Colorectal cancer (CRC) ranks as the third most prevalent cancer globally, and about half of CRC patients eventually succumb to tumor metastasis. Despite this, treatment options for metastatic colon cancer remain severely limited, reflected by a 12% 5-year overall survival rate. Increasing evidence suggests that cancer stem cells (CSCs) are pivotal in driving CRC metastasis. Our study found a significant upregulation of MOGS in metastatic colorectal cancer, with high MOGS expression inversely correlating with patient prognosis. Additionally, MOGS enhances the NOTCH pathway, thus promoting stemness in CRC cells, both in vitro and in vivo. Mechanistically, MOGS may facilitate the maturation of NOTCH1 protein by promoting NOTCH1 glycosylation. Correspondingly, silencing MOGS markedly reduced invasion and stemness of CRC cells *in vivo*. In summary, our findings highlight the critical role of MOGS in fostering stemness and activating the NOTCH pathway in colorectal cancer cells. Disrupting the function of the MOGS/NOTCH could represent a feasible therapeutic strategy for CRC management.

Keywords: MOGS, CRC stem cells, NOTCH pathway, protein glycosylation, prognostic biomarker

Introduction

Colorectal cancer (CRC) ranks as the third most common cancer worldwide [1]. Recent advancements in surgical techniques, chemotherapy, and molecular targeted drugs have improved the prognosis of patients with CRC. However, it remains the second leading cause of cancer-related deaths globally [2]. Alarmingly, about half of CRC patients succumb to tumor metastasis or recurrence [3]. The 5-year survival rate of colorectal cancer (CRC) is 64%, whereas the survival rate for metastatic CRC has plummeted to 12% [4]. Despite the development of various treatment modalities for CRC, including 5-fluorouracil, irinotecan, oxaliplatin-based chemotherapy, and anti-angiogenic or epidermal growth factor receptor-targeted therapies, therapeutic efficacy for metastatic colon cancer remains highly limited [5]. Thus, identifying potential therapeutic targets and understanding the molecular mechanisms involved in CRC

metastasis are of paramount clinical significance.

Cancer stem cells (CSCs), a small subpopulation within tumors, possess unique self-renewal and differentiation capabilities, making them one of critical drivers of the poor prognosis of malignant tumor [6]. In recent years, the investigation of CSCs in CRC has garnered substantial attention due to their involvement in tumor initiation, maintenance, recurrence, metastasis, and resistance to conventional therapies [7, 8]. Moreover, emerging evidence suggests that CSCs in CRC may exhibit dynamic plasticity, allowing them to transition between stem-like and differentiated states, contributing to tumor heterogeneity [9]. Stemness in cancer cells is regulated by multiple cellular pathways, including Wnt and Notch, among others [10, 11]. Recently, the Notch pathway has gained significant attention due to its multifaceted role in maintaining stemness and promoting oncogen-

esis [12-14]. Conventionally, the Notch pathway is activated through the interaction between Notch receptors (Notch1-4) and ligands (Jagged1, Jagged2, Delta-like 1, 3, and 4). Upon ligand-receptor engagement, proteolytic cleavage releases the Notch intracellular domain (NICD), which translocates to the nucleus to form a transcriptional activation complex [15]. This complex regulates the expression of downstream target genes, including stemness-related genes that promote tumor progression [10, 16, 17], and also affects the expression of downstream Hes and Hey family members, which function as transcription factors, further promoting the activation of oncogenes [18, 19].

MOGS (Mannosyl-Oligosaccharide Glucosidase) encodes the first enzyme in the N-linked oligosaccharide processing pathway, an essential step in glycosylation [20]. Glycosylation, the process of covalently attaching a carbohydrate to a target macromolecule, typically proteins and lipids, is mediated by the MOGS protein located in the endoplasmic reticulum lumen [21-23]. This protein cleaves the distal alpha-1,2-linked glucose residue from the Glc(3)-Man(9)-GlcNAc(2) oligosaccharide precursor, aiding in the modification and maturation of proteins and lipids [20]. MOGS has been reported to play a significant role in various pathophysiological processes, such as Alzheimer's disease and COVID-19 infection, etc. [24, 25]. However, the role and mechanisms of MOGS in colorectal cancer remain relatively understudied. A recent study using bioinformatics analysis revealed elevated MOGS expression in CRC tissues compared to normal tissues, with further support from Western blot and immunohistochemical assays [26]. These preliminary findings suggest a potential link between MOGS and colorectal cancer, highlighting the need for further research to elucidate this relationship and understand the functional implications.

Herein, we elucidate the significant implications of MOGS in the acquisition of stemness and invasion of colorectal cancer cells. Our findings demonstrate the upregulation of MOGS in CRC cells, facilitating the maturation of Notch1 protein, and leading to the activation of the Notch signaling pathway and the upregulation of stemness-related and invasion genes. This intricate mechanism underlines the role of MOGS in promoting stemness and invasion in

colorectal cancer. Consequently, our study highlights the crucial contribution of MOGS in colorectal cancer, suggesting its potential as a predictive biomarker and a promising therapeutic target for CRC patients.

Materials and methods

Cell culture and human tissue samples

Human colorectal cancer cell lines, including LOVO, HCT116, SW480, HCT15, RKO, CACO2, SW620, HCT8, LS174T, and DLD1, along with the normal colon mucosal epithelial cell line NCM460, were obtained from the American Type Culture Collection (ATCC). These cell lines were cultivated in RPMI 1640 medium (Gibco, Carlsbad, CA, USA), supplemented with 10% fetal bovine serum (FBS, Gibco, Carlsbad, CA, USA), and 100 IU/mL penicillin G, and 100 µg/mL streptomycin (Invitrogen Life Technologies, Carlsbad, CA, USA). The cells were maintained in a controlled environment at 37°C with 5% CO_2. Prior to experimentation, all cell lines underwent short tandem repeat (STR) profiling and received authentication certificates within the preceding four years. Experiments were conducted using cells propagated for less than six months post-resuscitation.

For Western blot analysis and immunohistochemical and immunofluorescence staining, 9 matched human CRC and normal tissue specimens were used. Additionally, 31 pairs of tissue specimens were sourced for qRT-PCR analysis from patients who underwent surgical treatment at Zhujiang Hospital between 2019 and 2023. The study protocol and informed consent procedure received ethical approval from the Ethical Committee of Southern Medical University. Expression profiling of target genes in CRC samples was conducted through a comprehensive search across TCGA COAD datasets and GEO repositories, including GSE21510, GSE38832, GSE41258, GSE17536, GSE8671, GSE166555, and GSE146771.

RNA isolation, reverse transcription, and quantitative real-time PCR

Total RNA was extracted from both cells and tissues using the RNAiso Plus reagent (Takara) following established protocols. To assess MOGS expression in colorectal cancer (CRC) cells and human tissue samples, isolated total

RNA underwent polyadenylation and reverse transcription (RT) using the Hifair®II 1st Strand cDNA Synthesis SuperMix (Yeasen, China). Real-time polymerase chain reaction (PCR) analysis was performed using the Hieff® qPCR SYBR® Green Master Mix (Low Rox Plus) kit (Yeasen, China). Experiments were conducted on an ABI 7500HT system according to the manufacturer's guidelines. The housekeeping gene GAPDH served as an internal normalizing control. All samples were standardized against internal controls. Quantification of fold change was calculated using the 2-ΔΔCT method. Specific primer sequences utilized are provided in Supplementary Table 1.

Western blot

Total protein extraction from cells or tissues was extracted using Radioimmunoprecipitation assay (RIPA) lysis buffer, supplemented with a cocktail of protease and phosphorylase inhibitors. Protein quantification was performed using the BCA protein assay kit (Pierce, KeyGEN BioTECH, Jiangsu, China). Proteins were separated by SDS-PAGE gel electrophoresis and transferred onto polyvinylidene fluoride (PVDF) membranes. Membrane blocking was performed using a Tris buffer with 0.1% Tween-20 and 5% nonfat milk at room temperature for 2 hours. PVDF membranes were then incubated overnight with primary antibodies specific to MOGS, NOTCH1, Hes1, CD133, SOX2, OCT4 (dilution: 1:1000; Proteintech Group, Inc., Chicago, IL, USA), and β-actin (dilution: 1:3000; Proteintech Group, Inc., Chicago, IL, USA). Following primary antibody incubation, membranes were treated with HRP-conjugated secondary antibodies (anti-rabbit IgG/anti-mouse IgG, dilution: 1:3000; Proteintech Group, Inc., Chicago, IL, USA) at room temperature for 2 hours. Protein signals were detected using an enhanced chemiluminescence detection system (Tennon5200, Shanghai, China), as per the manufacturer's guidelines.

Immunohistochemical staining

Surgical specimens from CRC patients and xenograft samples were fixed in 4% formalin, embedded in paraffin, and sectioned into 4 μm slices. Tissue sections underwent deparaffinization, dehydration, and incubation in 3% hydrogen peroxide for 10 minutes. Primary antibodies against Ki-67 (dilution: 1:300, Servi-cebio), and SOX2 (dilution: 1:200, Proteintech) were used for staining. After blocking with 5% BSA in PBS for 1 hour at room temperature, the sections were incubated with primary antibodies overnight at 4°C. This was followed by the application of corresponding secondary antibodies for 1 hour at room temperature. Target molecules were detected using DAB staining for immunohistochemistry, and slides were counterstained with hematoxylin. The intensity of staining in the immunostained sections was assessed by two independent pathologists.

Cell transfection

Small interfering RNAs (siRNAs) targeting MOGS (si-MOGS-1 & si-MOGS-2) and a scrambled oligonucleotide control (siRNA-NC) were obtained from GenePharma (Shanghai, China). Transfection into cells was performed using lipofectamine® 3000 reagent (Catalog Number: L3000015, Thermo Fisher Scientific, USA). Comprehensive details regarding the sequences of all siRNAs can be found in Supplementary Table 2. Lentivirus plasmids engineered to express MOGS or MOGS short hairpin RNA (shRNA) were constructed by Tsingke Biotechnology Co., Ltd. (Beijing, China). Cells were infected with lentivirus and polybrene for 24 hours. Cells stably expressing the vector, MOGS, or shMOGS were selected and maintained in culture medium supplemented with puromycin (2 μg/mL, Solarbio, China).

Cell counting kit-8 (CCK-8) assay and colony formation

For the CCK-8 assay, a total of 3000 cells after transfection were carefully seeded into each well of a 96-well plate, with a 100 μL volume of complete medium supplemented with 10% FBS and either DAPT or no DAPT. Each experimental condition was replicated in five separate wells. At designated time points (0, 24, 48, 72, and 96 hours) post incubation, 90 μL of RPMI 1640 and 10 μL of CCK-8 reagent (Dojindo Laboratory, Japan) were introduced into each well. The cells were then incubated for an additional 1.5 hours. Absorbance at 450 nm was measured using a microplate reader (Biotex, USA).

For the colony formation assay, post-transfection cells were seeded at a density of 2×10^3 cells per well in a six-well plate, with complete medium supplemented with 10% FBS and

either DAPT or no DAPT. After 14 days, the colonies were fixed with methanol and stained with a 0.1% crystal violet solution (Keygen, Nanjing, China).

Cell migration and invasion assay

Migration and invasion assays were conducted using cell culture inserts with 8-µm pores placed within 24-well plates (Costar, USA). For the invasion assay, the upper chamber was coated with 50 µL of Matrigel (BD Biosciences, San Jose, CA, USA), whereas for the migration assay, Matrigel coating was omitted. A total of 50,000 cells, suspended in 200 µL of serum-free medium with either DAPT or no DAPT, were seeded onto the upper chamber. Simultaneously, 0.6 mL of medium containing 20% FBS was added to the lower chamber to facilitate cell migration or invasion. After 24 or 48 hours of incubation at 37°C, cells that had migrated or invaded to the lower surface of the insert were fixed with methanol and stained with crystal violet; these cells were then visualized under a light microscope, and photographs of five randomly selected fields were captured for each condition to ensure comprehensive assessment.

In vivo tumor xenograft study

Subcutaneous xenograft colorectal cancer mouse model: HCT-116 cells stably transfected with Lentivirus-MOGS, Lentivirus-shMOGS or Lentivirus-vector control were suspended in fresh PBS at a concentration of $1×10^6$ cells/100 µL, and subcutaneously injected into Five-week-old Balb/c male nude mice, purchased from the Central Animal Facility of Southern Medical University. Each group consisted of 6 mice. Tumor growth was monitored every 6 days post-injection. After 24 days, mice were sacrificed, and tumor weight was measured. Xenografts were then fixed and sectioned for hematoxylin-eosin (HE) and immunohistochemical analysis. All protocols were approved by the Animal Care and Use Committee of Southern Medical University.

Orthotopic xenograft colorectal cancer mouse model: HCT-116 cells stably transfected with Lentivirus-shMOGS or Lentivirus-vector control were prepared and suspended in fresh PBS at a concentration of $1×10^6$ cells/50 µL. Six-week-old male BABL/c nude mice were obtained from

the Central Animal Facility of Southern Medical University. After anesthesia, a laparotomy was performed to expose the cecum, and 50 µL of the cell suspension was slowly injected into the cecal wall. Each group consisted of 6 mice. Care was taken to prevent leakage at the injection site. The cecum was then returned to the abdominal cavity, and the incisions were sutured. Moribund mice were euthanized, and orthotopic xenograft CRC masses were measured and harvested for further analysis. All procedures were approved by the Animal Care and Use Committee of Southern Medical University.

Tumorsphere formation assay

Cell suspensions were seeded in 6-well plates at a concentration of 5,000 cells/mL in a stem cell-conditioned medium consisting of DMEM/F12 supplemented with 100 IU/mL penicillin G, 100 µg/mL streptomycin, 10 ng/mL EGF (Peprotech Inc., Rocky Hill, NJ, USA), 10 ng/mL bFGF (Peprotech Inc., Rocky Hill, NJ, USA), and 1×B27 (Invitrogen). To assess the cellular response, images were captured from five randomly chosen regions within each experimental group, using a fluorescence microscope (Leica, Wetzlar, Germany). The number and diameter of the resulting cell spheres were analyzed. Only spheres with a diameter exceeding 50 µm were considered for analysis, providing a comprehensive evaluation of the cellular behavior.

In vitro limiting dilutions assay

Limiting dilution assays were conducted to determine the presence and frequency of sphere-forming cells. Cell suspensions were seeded at various dilutions, ranging from 30 to 1 cell per well, in a 96-well plate. Half of the media volume was replaced twice a week until day 21. The number of wells without spheres or semi-adherent cells was counted, and the ratio of these negative wells to the number of cells per well (cell dilution) was plotted to estimate the frequency of metasphere-initiating cells. The number of cells required to form a single sphere was determined based on the approach by Tropepe et al [27]. According to a Poisson distribution model, a fraction of 37% (corresponding to a fraction of 0.37) of negative wells indicated the dilution at which it was anticipated to have one metasphere-initiating cell (i.e., one sphere).

Statistical analysis

The data were analysed using SPSS version 20.0 software (SPSS, Chicago, IL, USA). Sample size for each study was chosen based on similar well-characterized experiments documented in the literature, with no statistical method used to predetermine sample size. Survival curves for Myo1b expression in CRC patients were analyzed using the Kaplan-Meier method and compared using the Log-rank test. Pearson's chi-squared (χ^2) test and unpaired Student's t-test were used to evaluate significance differences among groups. All statistical tests were two-sided. All data are presented as means ± SD (standard deviation).

Results

MOGS is highly expressed in CRC and predicts worse patient prognosis

To screen candidate genes associated with CRC occurrence and progression, we first performed differentially expressed gene (DEG) analysis on the GSE21250 dataset. We compared gene expression profiles between CRC and normal colon tissues, as well as between metastatic CRC (mCRC) and non-metastatic CRC (nmCRC) tissues. Following the DEG analysis, genes with |logFC| > 0 and *P* values < 0.05 were identified as DEGs (**Figure 1A**, Supplementary Figure 1A). Among these, 826 upregulated DEGs, including MOGS, were identified. We then conducted a univariate Cox analysis to determine which genes functioned as independent predictors in CRC, identifying 7 genes, including MOGS. As listed in **Figure 1B**, univariate Cox analysis revealed that high MOGS expression was significantly correlated with poor overall survival (hazard ratio [HR] = 2.943, 95% CI = 1.231-2.139, P < 0.001). Kaplan-Meier analyses of the other six genes are presented in Supplementary Figure 1B. Protein expression levels of MOGS in 9 pairs of primary CRC tissue and matched adjacent normal tissue were detected by western blot and IHC assays, showing significantly higher MOGS expression in CRC tissues compared to matched adjacent normal mucosa (**Figure 1C** and **1D**). We also observed significantly higher transcriptional levels of MOGS in CRC tissues than in normal mucosa in the TCGA-COAD dataset (**Figure 1E**, left panel) and among 32 pairs of CRC tissues and matched normal mucosa

samples from the Zhujiang cohort (**Figure 1E**, right panel). Further investigation of MOGS expression in CRC samples with different tumor stages revealed dramatically higher expression in samples with higher stages (**Figure 1F**). Similar results were found in TCGA-COAD samples with different N and M stages (**Figure 1G**). MOGS was also upregulated in liver and lung metastasis tumors compared to primary CRC tissues (**Figure 1H**). Moreover, high MOGS expression in tumor tissues indicated a poor prognosis for CRC patients (**Figure 1I**). These findings suggest that MOGS may significantly impact CRC tumorigenicity and metastatic potential.
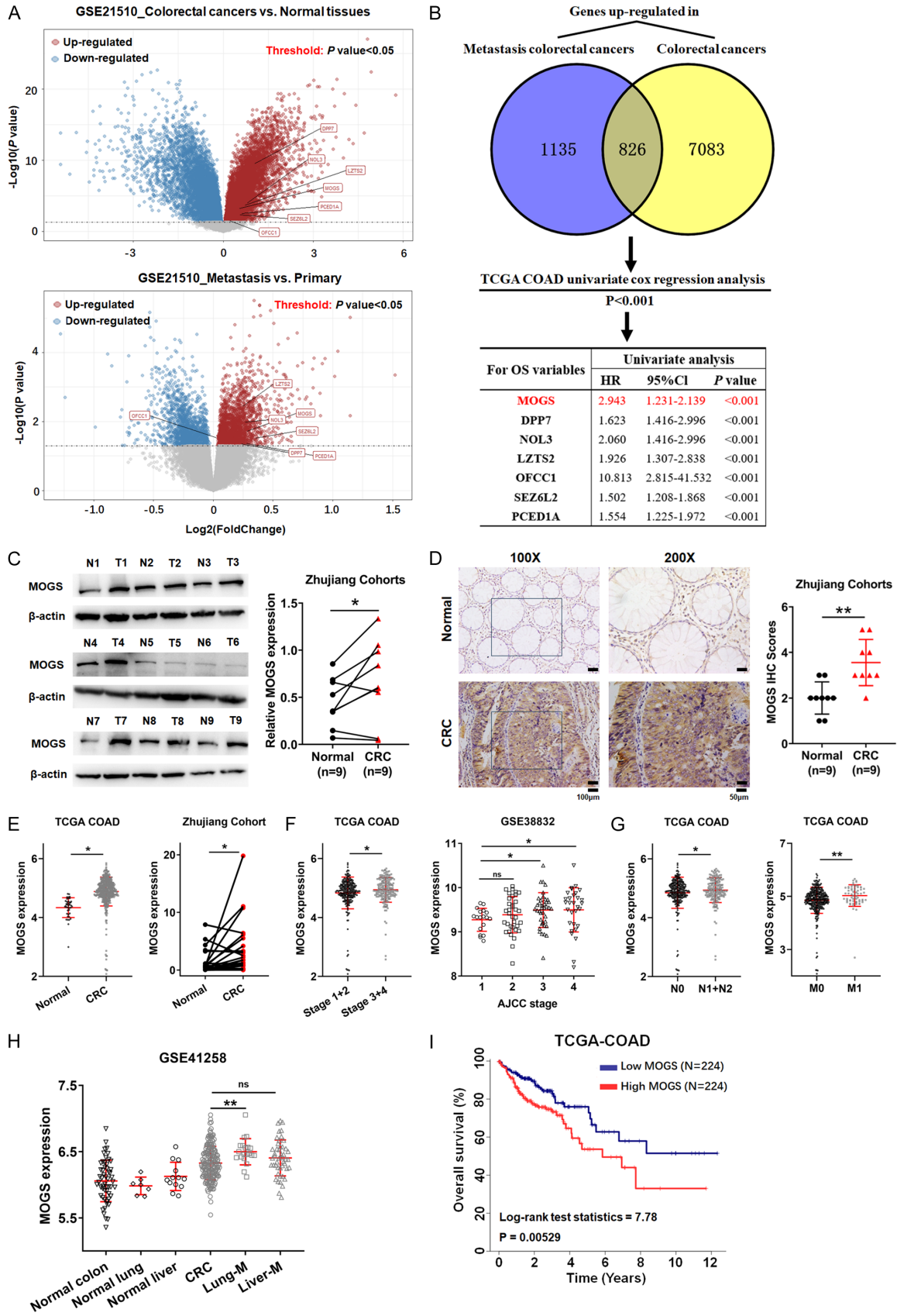
MOGS promotes the migration, invasion and proliferation properties of CRC cells in vitro

In an in vitro study, we examined the transcriptional level of MOGS in 11 CRC cell lines (SW480, RKO, SW620, HCT116, LS174T, LOVO, CACO2, DLD1, HCT15, HCT8 and HT29) and one normal epithelial cell line (NCM460) (**Figure 2A**). Gain- and loss-of-function analyses were conducted in two cell lines; these cell lines (HCT116 and DLD1) were chosen for subsequent experiments due to moderate MOGS expression. MOGS expression in both HCT116 (**Figure 2B**) and DLD1 (**Figure 2C**) cell lines was modulated either by transducing with a lentivirus driving MOGS overexpression (Lv-MOGS) through transgene delivery or MOGS knockdown by short hairpin RNA (shMOGS). Western blot and RT-qPCR assays were conducted to verify transduction efficacy. Transwell (**Figure 2D**, **2E**) and tumor invasion (**Figure 2F**, **2G**) assays revealed that MOGS significantly enhanced the migration and invasion potential of both HCT116 and DLD1 cells. Colony formation assay (**Figure 2H**, **2I**) and CCK-8 assay (Supplementary Figure 2) further showed that MOGS markedly promoted cell proliferation in CRC cells. Taken together, our study reveals that MOGS has a significant effect on CRC proliferation, migration, and invasion, though the underlying mechanisms remain largely unknown.

MOGS promotes CRC stemness via activating NOTCH pathway in vitro

To identify the oncogenic signaling pathways related to MOGS, we applied GSEA analysis to CRC specimens from four GEO datasets respec-

A GSE21510_Colorectal cancers vs. Normal tissues

GSE21510_Metastasis vs. Primary

B Genes up-regulated in

Metastasis colorectal cancers / Colorectal cancers

TCGA COAD univariate cox regression analysis

P<0.001

For OS variables	Univariate analysis		
	HR	95%CI	*P* value
MOGS	2.943	1.231-2.139	<0.001
DPP7	1.623	1.416-2.996	<0.001
NOL3	2.060	1.416-2.996	<0.001
LZTS2	1.926	1.307-2.838	<0.001
OFCC1	10.813	2.815-41.532	<0.001
SEZ6L2	1.502	1.208-1.868	<0.001
PCED1A	1.554	1.225-1.972	<0.001

C Zhujiang Cohorts

D Zhujiang Cohorts

E TCGA COAD / Zhujiang Cohort

F TCGA COAD / GSE38832

G TCGA COAD / TCGA COAD

H GSE41258

I TCGA-COAD

Low MOGS (N=224)
High MOGS (N=224)

Log-rank test statistics = 7.78
P = 0.00529

Figure 1. Upregulation of MOGS in CRC is tightly associated with tumor metastasis and poor prognosis of patients. A. The above volcano plots represent differential expression changes between CRC samples and normal samples from GSE21510 dataset. The below volcano plots represent differential expression changes between metastatic CRC samples and primary CRC samples from GSE21510 dataset. The X-axis indicates log2 fold changes (FC), and the Y-axis indicates the negative logarithm (base 10) of the adjusted *p*-values. Gray vertical and horizontal dashed lines denote the filtering criteria. Red and blue dots represent genes expressed at significantly higher or lower levels, respectively. B. Identification of candidate prognosis-related genes in TCGA COAD cohorts by univariate COX regression analysis. C. Immunoblot for MOGS protein expression in 9 human CRC tissues and matched adjacent normal tissues from the same patient. Quantification of protein levels, normalized to β-actin, is shown in the right panel. D. Representative MOGS IHC images of adjacent normal tissue and tumor tissue (n = 9) sample. IHC scores are displayed in the right panel. E. Scatter diagram represents MOGS expression level of human normal tissues and CRC tissues from TCGA cohort (left panel) and Zhujiang Hospital (right panel). F. Left panel represents the difference in MOGS expression between stage 1/2 and stage 3/4 CRC samples from TCGA cohort. The right panel shows the difference in MOGS expression among AJCC stages 1 to 4 CRC samples from the GEO: GSE38832 dataset. G. The left panel represents the difference in MOGS expression between N0 and N1/2 CRC samples from the TCGA cohort. The right panel represents the difference in MOGS expression between M0 and M1 CRC samples from TCGA cohort. H. Scatter diagram represents MOGS expression level of primary colon adenocarcinomas, adenomas, metastases, and corresponding normal mucosae. I. Kaplan-Meier survival analysis in COAD samples from TCGA cohort. *$P <$ 0.05, **$P <$ 0.01, ***$P <$ 0.001.

tively (GSE39582, GSE83889, GSE17536, and GSE8671). A total of one overlapping pathway was positively enriched in specimens with high MOGS expression compared to those with low expression, indicating a strong correlation between MOGS and the NOTCH pathway (**Figure 3A**). Enrichment plots are shown in Supplementary Figure 3. Given the close correlation between NOTCH pathway and cancer stem cells (CSCs), we hypothesized that MOGS might promote CRC progression via NOTCH pathway-mediated tumor stemness. Western blot assays confirmed that MOGS significantly increased the expression levels of NOTCH1 and HES1, key indicators of NOTCH pathway activity. In addition, stemness markers such as CD133, OCT4, and SOX2 were upregulated with MOGS overexpression. Conversely, silencing MOGS in HCT116 and DLD1 cells led to systematic knockdown (**Figure 3B**). In vitro limiting dilution assays were conducted to investigate the role of MOGS in maintaining stemness. **Figure 3C** shows that MOGS knockdown significantly inhibited the self-renewal capacity of HCT116 and DLD1 cells, whereas self-renewal was enhanced by MOGS overexpression. Furthermore, smaller sized and fewer CSC spheres were formed in MOGS knockdown cells (**Figure 3E** and **3G**), while more and larger spheres formed after upregulating MOGS (**Figure 3D** and **3F**). Interestingly, when analyzing MOGS expression across various cell types in scRNA-seq datasets, we found that NOTCH1 and HES1 expression levels were significantly lower in CRC tissues with low MOGS expression (GSE146771), but significantly higher in tissues

with high MOGS expression (GSE166555) (**Figure 3H**).

MOGS promotes CRC tumorigenicity and progression in vivo

In vivo limiting dilution assays and an orthotopic xenograft CRC mouse model were employed to evaluate the effect of MOGS on CRC stemness in vivo. As illustrated in **Figure 4A-C**, MOGS knockdown significantly inhibited the tumorigenicity and proliferation of CRC cells. In the orthotopic xenograft CRC mice model, silencing MOGS not only restricted tumor growth (**Figure 4D**), but also prolonged the survival of tumor-bearing mice (**Figure 4E**). Immunohistochemical assays revealed a marked decrease in the expression levels of the proliferation marker Ki67 and CSC marker SOX2 in MOGS-knockdown tumors compared to control tumors (**Figure 4F**). Therefore, MOGS disruption suppressed CRC progression in vivo and improved the prognosis in this model.

Inhibiting NOTCH pathway markedly rescue the MOGS-mediated metastasis and stemness of CRC cells both in vitro and in vivo

To elucidate the role of NOTCH pathway in MOGS-mediated stemness and metastasis of CRC cells, we disrupted the pathway in MOGS-overexpressing (MOGS-OE) HCT116 and DLD1 cells using DAPT, a NOTCH pathway inhibitor. Transwell (**Figure 5A**) and CCK8 (**Figure 5B**) assays demonstrated that disrupting the NOTCH pathway significantly eliminated the promotion of MOGS in CRC cell migration and
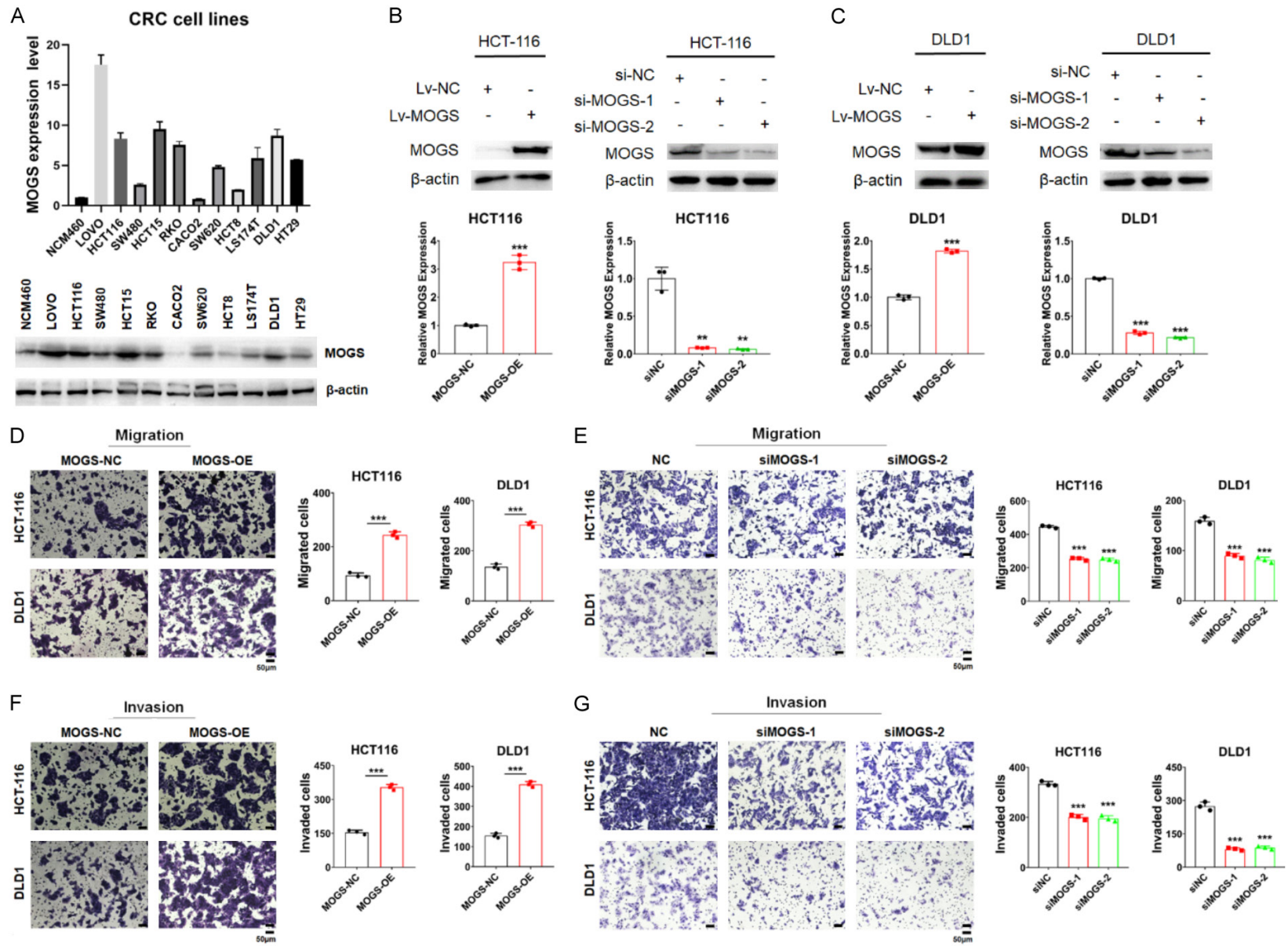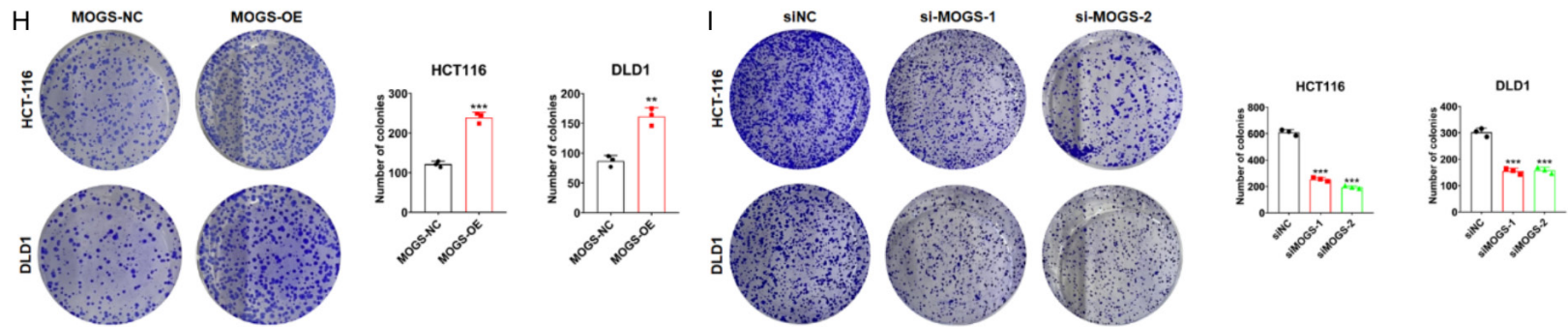
Figure 2. MOGS promotes the migration, invasion and proliferation properties of CRC cells *in vitro*. (A) Expression of MOGS mRNA (top panel) and protein (bottom-panel) was detected in NCM460 and 11 different CRC cell lines. (B, C) Western blot and RT-qPCR assay were used to verify transduction efficacy of MOGS overexpression and knockdown in HCT-116 (B) and DLD1 cells (C). (D, E) Transwell assay for migration properties of MOGS overexpression (D) and knockdown (E) cells. Data are expressed as means ± SD. (F, G) Transwell assay for cell invasion properties of MOGS overexpression (F) and knockdown (G) cells. Data are expressed as means ± SD. (H, I) Representative images of colony formation assays; bars in the right panel reflect means ± SD. *$P < 0.05$, **$P < 0.01$, ***$P < 0.001$.
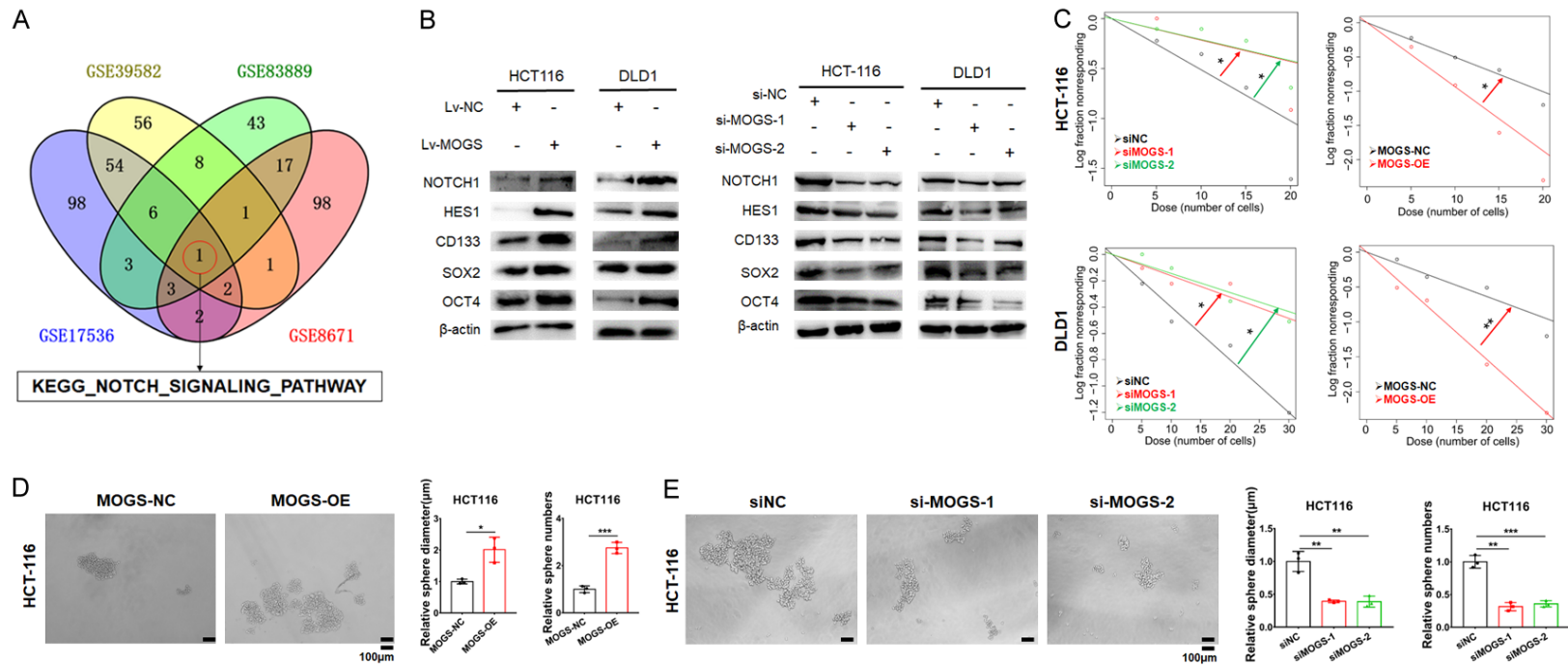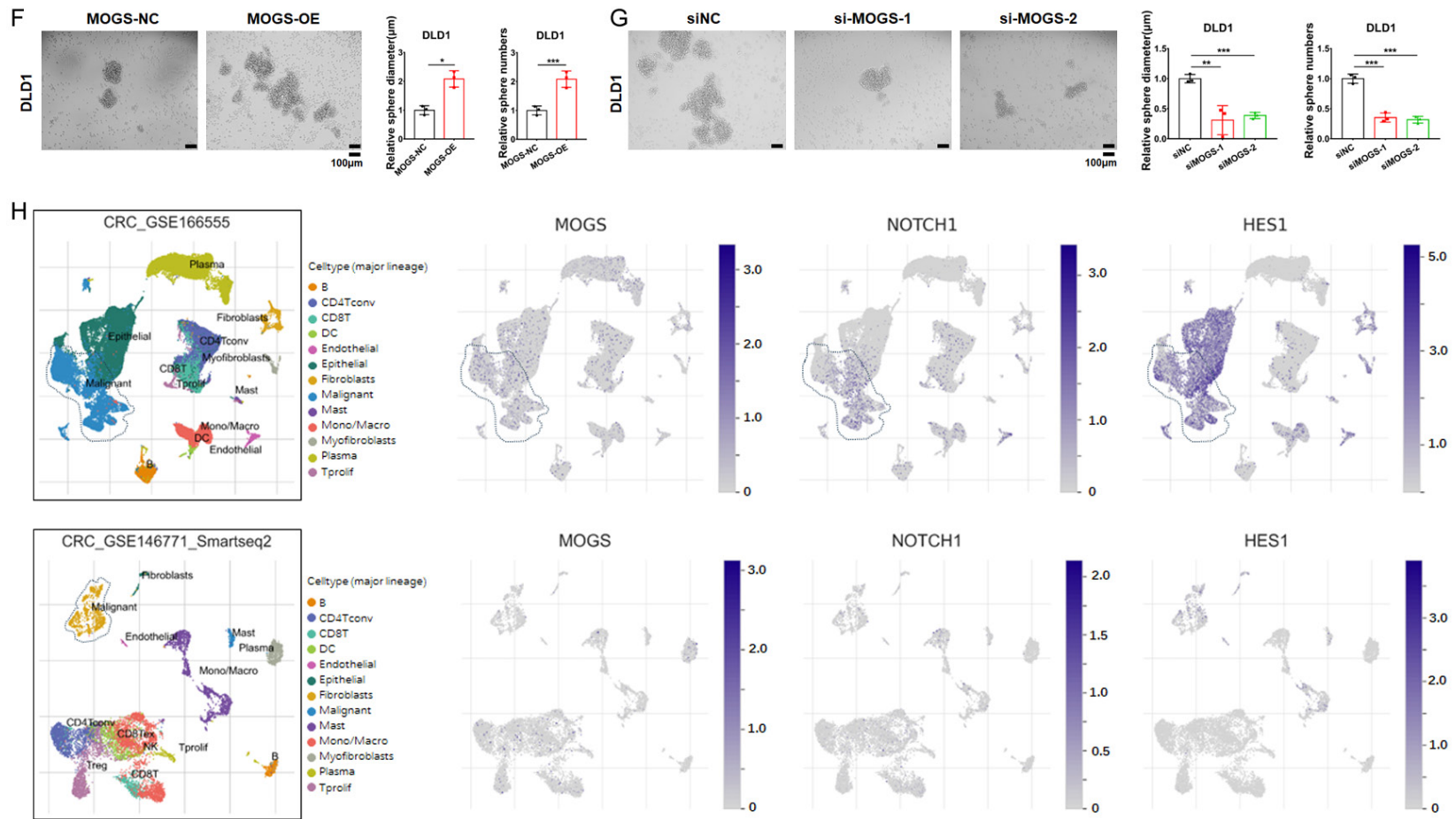
Figure 3. MOGS promotes the stemness properties of CRC cells via activating NOTCH pathway *in vitro*. A. GSEA was performed to compare high MOGS and low MOGS expression groups in four published CRC gene expression profiles (GSE39582, GSE83889, GSE17536 and GSE8671). The four-way Venn diagram illustrates the enrichment results in each dataset, with gene sets common to all datasets extracted. B. Representative Western blots for NOTCH pathway markers (NOTCH1 and HES1) and stemness-associated genes (CD133, SOX2 and OCT4). C. The *in vitro* limiting dilution assay demonstrates the effects of MOGS on the formation of CSC spheres, as assessed by the likelihood ratio test. D-G. Representative images of sphere formation assay; bars in the right panel represent means ± SD. H. Expression pattern of MOGS, NOTCH1 and HES1 in CRC scRNA-seq data from GEO: GSE166555 and GSE166771 dataset. *P < 0.05, **P < 0.01, ***P < 0.001.
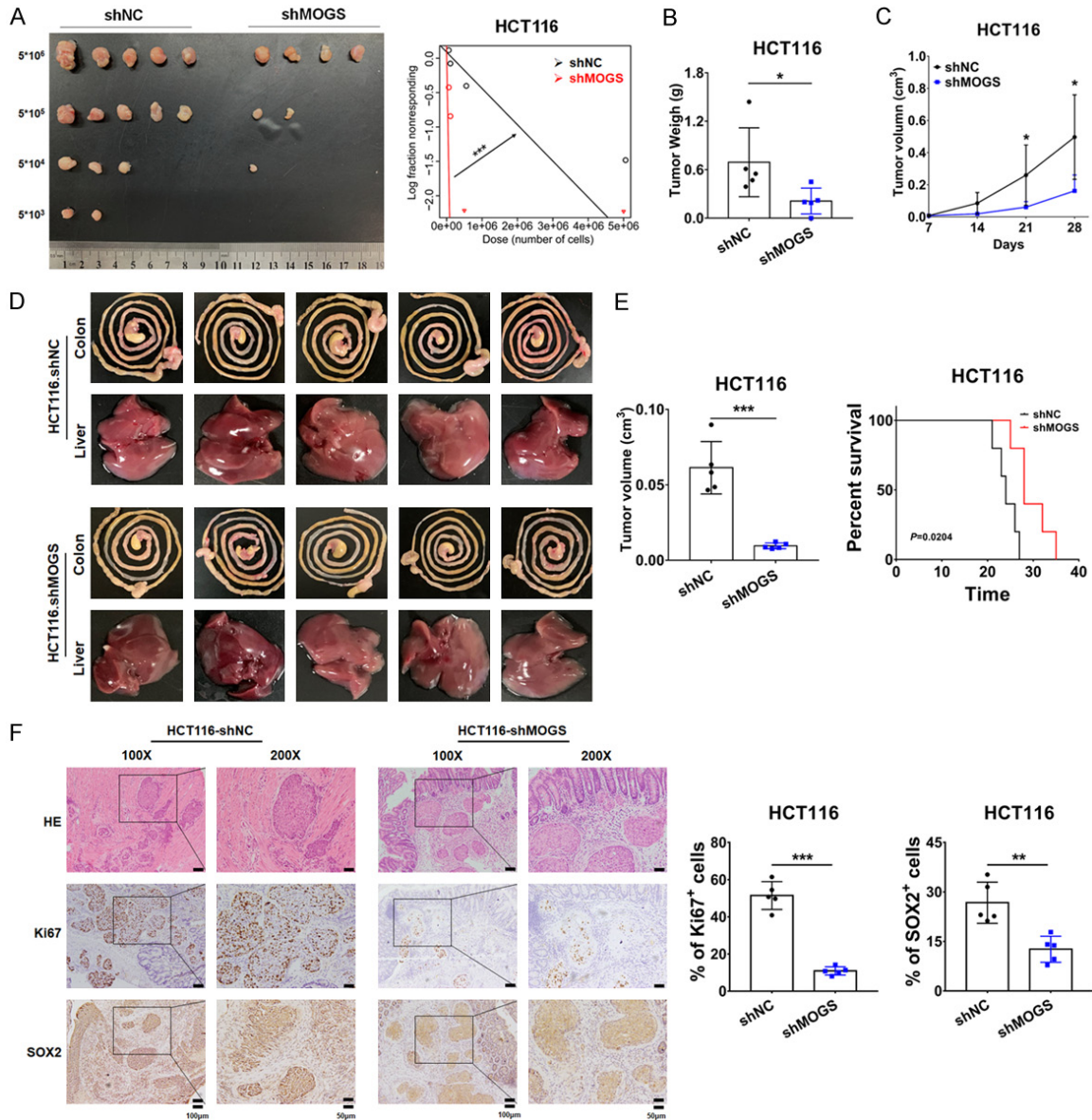
Figure 4. Knockdown of MOGS potently inhibits CRC proliferation, stemness and prolongs the animal survival in Orthotopic xenograft models. (A) *In vivo* limiting dilution analysis was conducted to assess the tumorigenicity of shNC and shMOGS CRC cells in nude mice (mean ± SD, n = 5). (B, C) Subcutaneous tumors formed by control and MOGS-silenced HCT116 cells (5*10⁶ cells per mouse) were harvested from nude mice. Both the weight (B) and volume (C) of subcutaneous tumors are shown in the right panel (mean ± SD, n = 5). (D) Orthotopic xenograft colorectal cancer mouse model. The specified cells were injected into the intestinal serous cavities of nude mice. n = 5 for each group. (E) The left panel shows the tumor volume for each group. The right panel presents Kaplan-Meier survival analysis of mice bearing xenografts, n = 5 for each group. (F) Paraffin-embedded xenograft sections were stained with antibodies targeting human SOX2 and Ki67. *$P < 0.05$, **$P < 0.01$, ***$P < 0.001$.

proliferation. Further studies also revealed that inhibiting the NOTCH pathway significantly diminished the sphere-forming properties of CRC cells, which were enhanced by MOGS overexpression (**Figure 5C** and **5D**). Consistent with these biological phenotypes, weakening the NOTCH pathway substantially reversed the alterations in stemness signatures (SOX2, CD133, and OCT4) and NOTCH signaling (NOTCH1 and HES1) mediated by MOGS (**Figure 5E**).

Moreover, inhibition of NOTCH pathway also significantly reversed the accelerated tumor
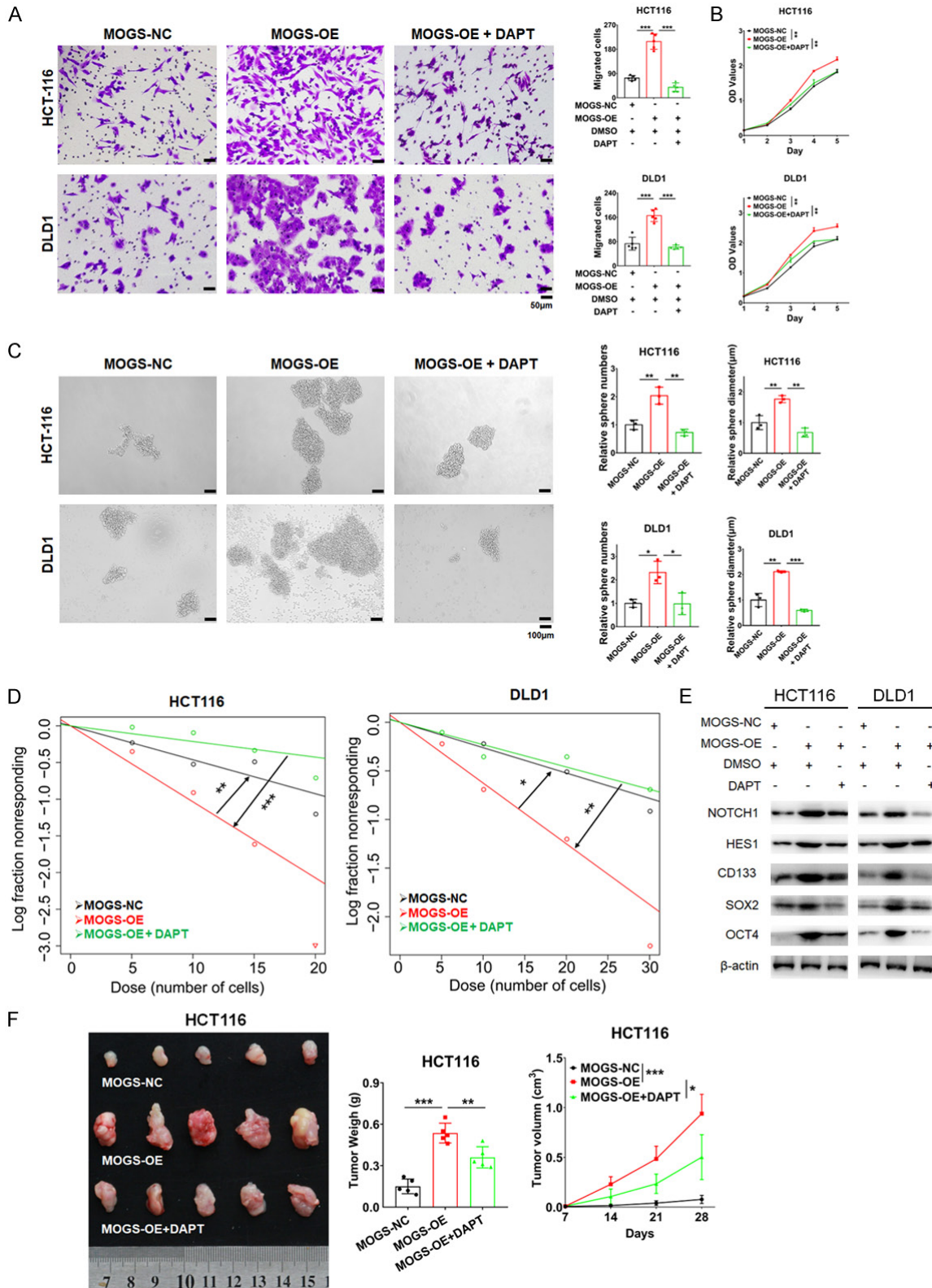
Figure 5. MOGS/NOTCH1/HES1 axis plays a critical role in MOGS-mediated metastasis and stemness. (A) Transwell assays illustrate the effects of the NOTCH pathway inhibitor DAPT on MOGS-mediated migration of CRC cells. (B) CCK-8 assay show the effects of DAPT on MOGS-mediated proliferation of CRC cells. (C, D) Sphere formation assay (C) and *in vitro* limiting dilution assay (D) demonstrate the effects of DAPT on MOGS-mediated stemness of CRC cells. (E) Effects of DAPT on the expression of stemness markers (CD133, SOX2, and OCT4) and NOTCH pathway proteins (NOTCH1 and HES1) modulated by MOGS in CRC cells. (F) Effects of DAPT on the growth of subcutaneous tumors facilitated by MOGS overexpression in HCT-116 cells. Both the weight and volume of subcutaneous tumors are shown in the right panel (mean ± SD, n = 5). *$P < 0.05$, **$P < 0.01$, ***$P < 0.001$.
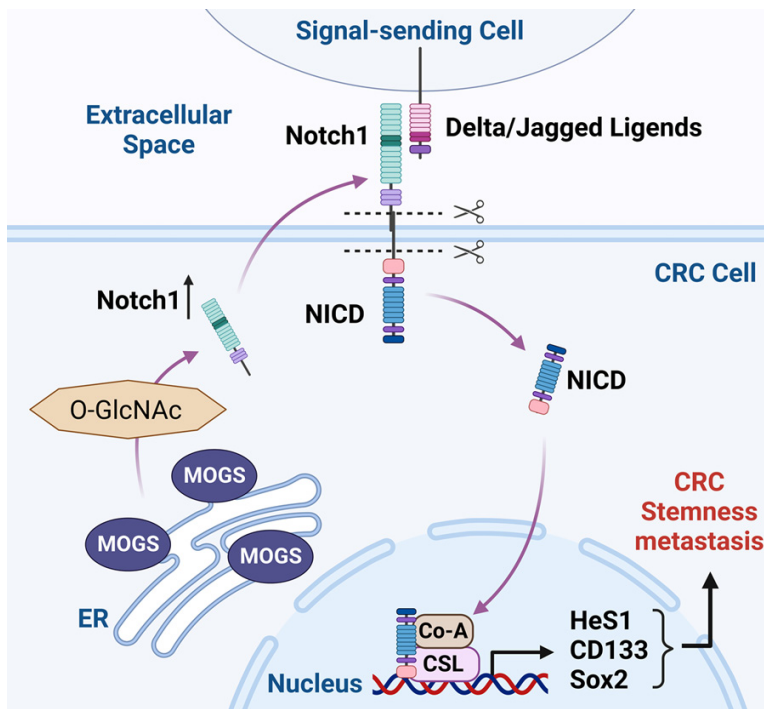
Figure 6. Graphical abstract of the mechanism in this study.

growth induced by MOGS overexpression in a subcutaneous tumor model (**Figure 5F**). Taken together, these findings suggest that MOGS primarily promotes stemness and migration of CRC cells via the NOCTH1/HES1 axis.

Discussion

Colorectal cancer (CRC) is the third most common cancer and the second leading cause for cancer-related death worldwide [2, 28, 29]. Despite significant advances in treatment modalities, tumor metastasis remains a significant challenge. Postoperative local recurrence and distant metastasis are critical factors constraining the prognosis of CRC patients [5, 30, 31]. However, the molecular mechanisms underlying the metastasis and recurrence of CRC remain unclear [5]. In the present study, we identified the involvement of MOGs in the acquisition of stemness and metastasis in CRC.

Cancer stem cells (CSCs), a small subset of cells within a tumor that can withstand treatment and possess the ability for multiple differentiations, play a crucial role in various aspects such as drug resistance and recurrence [6, 32]. CSCs are key contributors to local

recurrence and distant metastasis in CRC, signifying that targeting tumor stem cells presents a promising and novel avenue for CRC treatment. However, clinical research directly targeting tumor stem cells and their associated molecular pathways is relatively scarce [7]. For CRC, clinical Phase III trials for napabucasin (an inhibitor of the tumor stem cell marker DLL4), both as a standalone treatment (NCT-035222649) and in combination with the FOLFIR regimen (NCT02752127), are currently underway. A thorough exploration of tumor stem cell markers and their regulatory mechanisms will provide a theoretical foundation and methodology for targeting CRC stem cells. Our study reveals that MOGS mediates enhanced stemness in CRC, promoting malignant progression. To further elucidate the mechanisms by which MOGS regulates tumor stem cells, we conducted comprehensive analyses across multiple databases and validated our findings through experimental studies. Our findings indicate that MOGS is involved in the activation of the NOTCH pathway in CRC. One of the most critical characteristics of tumor stem cells is the abnormal activation and alteration of signaling pathways such as Notch, SHH, NF-κB, and Wnt, which lead to rapid proliferation, pluripotent differentiation, self-renewal, and drug resistance. To confirm whether the NOTCH signaling pathway mediates the pathological role of MOGS in CRC cells, we used DAPT, a NOTCH signaling pathway inhibitor, to selectively inhibit NOTH both in vivo and in vitro. Assay results confirmed that MOGS promoted tumor cell metastasis and stemness by activating the NOTCH signaling pathway.

MOGS, a protein located in the endoplasmic reticulum, is involved in the glycosylation process of various proteins, which assumes a pivotal role in the maturation of various proteins [20, 25, 33]. Previous studies have shown that NOTCH1 protein, the key receptor in the NOTCH

pathway, requires glycosylation and maturation before transportation to the cell membrane and subsequent receptor function [34]. Based upon this insight, we hypothesize that MOGS promotes the activation of the NOTCH pathway by mediating the glycosylation of NOCTH1 protein.

There are, however, some limitations to our research. Although our study demonstrated that MOGS promotes the activation of NOTCH signaling pathway in CRC cells, which upregulates the expression of downstream targets initiating cancer cell metastasis and enhanced stemness, the underlying molecular mediators of MOGS-driven NOTCH pathway activation, necessitate further elucidation. Whether the effector molecules of cancer cell metastasis and stemness acquisition are activated by the NICD transcription factor complex or the Hes1 transcription factor remains to be explored.

In conclusion, our findings indicate that MOGS are pivotal drivers of stemness acquisition and metastasis in CRC. Through in vivo and in vitro experiments, we discovered that MOGS mediates the glycosylation of NOTCH1 protein and activates the NOTCH pathway, enhancing the acquisition of stemness and metastasis in CRC cells (**Figure 6**). Therefore, targeting MOGS may be an effective treatment strategy for CRC.

Acknowledgements

Disclosure of conflict of interest

None.

Address correspondence to: Kehong Zheng and Lang Xie, Department of General Surgery, Zhujiang Hospital, Southern Medical University, Guangzhou 510280, Guangdong, China. E-mail: drzheng-kh@163.com (KHZ); langxiezj@hotmail.com (LX)

References

[1] Sung H, Ferlay J, Siegel RL, Laversanne M, Soerjomataram I, Jemal A and Bray F. Global cancer statistics 2020: GLOBOCAN estimates of incidence and mortality worldwide for 36 cancers in 185 countries. CA Cancer J Clin 2021; 71: 209-249.

[2] Siegel RL, Wagle NS, Cercek A, Smith RA and Jemal A. Colorectal cancer statistics, 2023. CA Cancer J Clin 2023; 73: 233-254.

[3] Chen W, Zheng R, Baade PD, Zhang S, Zeng H, Bray F, Jemal A, Yu XQ and He J. Cancer statistics in China, 2015. CA Cancer J Clin 2016; 66: 115-132.

[4] Siegel RL, Miller KD and Jemal A. Cancer statistics, 2019. CA Cancer J Clin 2019; 69: 7-34.

[5] Tsilimigras DI, Ntanasis-Stathopoulos I and Pawlik TM. Molecular mechanisms of colorectal liver metastases. Cells 2023; 12: 1657.

[6] Zheng XX, Chen JJ, Sun YB, Chen TQ, Wang J and Yu SC. Mitochondria in cancer stem cells: achilles heel or hard armor. Trends Cell Biol 2023; 33: 708-727.

[7] Ebrahimi N, Afshinpour M, Fakhr SS, Kalkhoran PG, Shadman-Manesh V, Adelian S, Beiranvand S, Rezaei-Tazangi F, Khorram R, Hamblin MR and Aref AR. Cancer stem cells in colorectal cancer: signaling pathways involved in stemness and therapy resistance. Crit Rev Oncol Hematol 2023; 182: 103920.

[8] Xuan SH, Hua ML, Xiang Z, He XL, Huang L, Jiang C, Dong P and Wu J. Roles of cancer stem cells in gastrointestinal cancers. World J Stem Cells 2023; 15: 209-220.

[9] Clara JA, Monge C, Yang Y and Takebe N. Targeting signalling pathways and the immune microenvironment of cancer stem cells - a clinical update. Nat Rev Clin Oncol 2020; 17: 204-232.

[10] Yang L, Shi P, Zhao G, Xu J, Peng W, Zhang J, Zhang G, Wang X, Dong Z, Chen F and Cui H. Targeting cancer stem cell pathways for cancer therapy. Signal Transduct Target Ther 2020; 5: 8.

[11] Chen Z, Chen Y, Li Y, Lian W, Zheng K, Zhang Y, Zhang Y, Lin C, Liu C, Sun F, Sun X, Wang J, Zhao L and Ke Y. Prrx1 promotes stemness and angiogenesis via activating TGF-beta/smad pathway and upregulating proangiogenic factors in glioma. Cell Death Dis 2021; 12: 615.

[12] Fu W, Li G, Lei C, Qian K, Zhang S, Zhao J and Hu S. Bispecific antibodies targeting EGFR/Notch enhance the response to talazoparib by decreasing tumour-initiating cell frequency. Theranostics 2023; 13: 3641-3654.

[13] Yang L, Yang M, Cui C, Long X, Li Y, Dai W, Lang T and Zhou Q. The myo-inositol biosynthesis rate-limiting enzyme ISYNA1 suppresses the stemness of ovarian cancer via Notch1 pathway. Cell Signal 2023; 107: 110688.

[14] Kim EJ, Kim JY, Kim SO, Hong N, Choi SH, Park MG, Jang J, Ham SW, Seo S, Lee SY, Lee K, Jeong HJ, Kim SJ, Jeong S, Min K, Kim SC, Jin X, Kim SH, Kim SH and Kim H. The oncogenic JAG1 intracellular domain is a transcriptional

cofactor that acts in concert with DDX17/SMAD3/TGIF2. Cell Rep 2022; 41: 111626.

[15] Kopan R and Ilagan MX. The canonical Notch signaling pathway: unfolding the activation mechanism. Cell 2009; 137: 216-233.

[16] Jin Y, Jung SN, Lim MA, Oh C, Piao Y, Kim HJ, Nguyena Q, Kang YE, Chang JW, Won HR and Koo BS. SHMT2 induces stemness and progression of head and neck cancer. Int J Mol Sci 2022; 23: 9714.

[17] Wang LL, Wan XY, Liu CQ and Zheng FM. NDR1 increases NOTCH1 signaling activity by impairing Fbw7 mediated NICD degradation to enhance breast cancer stem cell properties. Mol Med 2022; 28: 49.

[18] Riya PA, Basu B, Surya S, Parvathy S, Lalitha S, Jyothi NP, Meera V, Jaikumar VS, Sunitha P, Shahina A, Sukumaran R, Nair AS, Dhanesh SB, Jiffy J, Nelson-Sati S, Maliekal TT, Das AV and James J. HES1 promoter activation dynamics reveal the plasticity, stemness and heterogeneity in neuroblastoma cancer stem cells. J Cell Sci 2022; 135: jcs260157.

[19] Katoh M and Katoh M. Integrative genomic analyses on HES/HEY family: Notch-independent HES1, HES3 transcription in undifferentiated ES cells, and Notch-dependent HES1, HES5, HEY1, HEY2, HEYL transcription in fetal tissues, adult tissues, or cancer. Int J Oncol 2007; 31: 461-466.

[20] Sadat MA, Moir S, Chun TW, Lusso P, Kaplan G, Wolfe L, Memoli MJ, He M, Vega H, Kim LJY, Huang Y, Hussein N, Nievas E, Mitchell R, Garofalo M, Louie A, Ireland DC, Grunes C, Cimbro R, Patel V, Holzapfel G, Salahuddin D, Bristol T, Adams D, Marciano BE, Hegde M, Li Y, Calvo KR, Stoddard J, Justement JS, Jacques J, Priel DAL, Murray D, Sun P, Kuhns DB, Boerkoel CF, Chiorini JA, Di Pasquale G, Verthelyi D and Rosenzweig SD. Glycosylation, hypogammaglobulinemia, and resistance to viral infections. N Engl J Med 2014; 370: 1615-1625.

[21] Lin B, Qing X, Liao J and Zhuo K. Role of protein glycosylation in host-pathogen interaction. Cells 2020; 9: 1022.

[22] Eichler J. Protein glycosylation. Curr Biol 2019; 29: R229-R231.

[23] Maccioni HJ. Glycosylation of glycolipids in the Golgi complex. J Neurochem 2007; 103 Suppl 1: 81-90.

[24] Suzuki M, Tezuka K, Handa T, Sato R, Takeuchi H, Takao M, Tano M and Uchida Y. Upregulation of ribosome complexes at the blood-brain barrier in Alzheimer's disease patients. J Cereb Blood Flow Metab 2022; 42: 2134-2150.

[25] Nunes-Santos CJ, Kuehn HS and Rosenzweig SD. N-Glycan modification in Covid-19 pathophysiology: in vitro structural changes with limited functional effects. J Clin Immunol 2021; 41: 335-344.

[26] Chen Y, Lu Y, Huang C, Wu J, Shao Y, Wang Z, Zhang H and Fu Z. Subtypes analysis and prognostic model construction based on lysosome-related genes in colon adenocarcinoma. Front Genet 2023; 14: 1149995.

[27] Tropepe V, Sibilia M, Ciruna BG, Rossant J, Wagner EF and van der Kooy D. Distinct neural stem cells proliferate in response to EGF and FGF in the developing mouse telencephalon. Dev Biol 1999; 208: 166-188.

[28] Chen YH, Xu NZ, Hong C, Li WQ, Zhang YQ, Yu XY, Huang YL and Zhou JY. Myo1b promotes tumor progression and angiogenesis by inhibiting autophagic degradation of HIF-1alpha in colorectal cancer. Cell Death Dis 2022; 13: 939.

[29] Zheng K, Zhou X, Yu J, Li Q, Wang H, Li M, Shao Z, Zhang F, Luo Y, Shen Z, Chen F, Shi F, Cui C, Zhao D, Lin Z, Zheng W, Zou Z, Huang Z and Zhao L. Epigenetic silencing of miR-490-3p promotes development of an aggressive colorectal cancer phenotype through activation of the Wnt/beta-catenin signaling pathway. Cancer Lett 2016; 376: 178-187.

[30] Zheng K, Yu J, Chen Z, Zhou R, Lin C, Zhang Y, Huang Z, Yu L, Zhao L and Wang Q. Ethanol promotes alcohol-related colorectal cancer metastasis via the TGF-beta/RUNX3/Snail axis by inducing TGF-beta1 upregulation and RUNX3 cytoplasmic mislocalization. EBioMedicine 2019; 50: 224-237.

[31] Biller LH and Schrag D. Diagnosis and treatment of metastatic colorectal cancer: a review. JAMA 2021; 325: 669-685.

[32] Chen Z, Zhang Y, Chen Y, Lin W, Zhang Y, Cai G, Sun X, Zheng K, He J, Ai T, Wang J, Zhao L and Ke Y. Prrx1 promotes resistance to temozolomide by upregulating ABCC1 and inducing vasculogenic mimicry in glioma. Am J Cancer Res 2022; 12: 3892-3912.

[33] Liu Y, Leslie PL, Jin A, Itahana K, Graves LM and Zhang Y. p32 regulates ER stress and lipid homeostasis by down-regulating GCS1 expression. FASEB J 2018; 32: 3892-3902.

[34] Pakkiriswami S, Couto A, Nagarajan U and Georgiou M. Glycosylated notch and cancer. Front Oncol 2016; 6: 37.

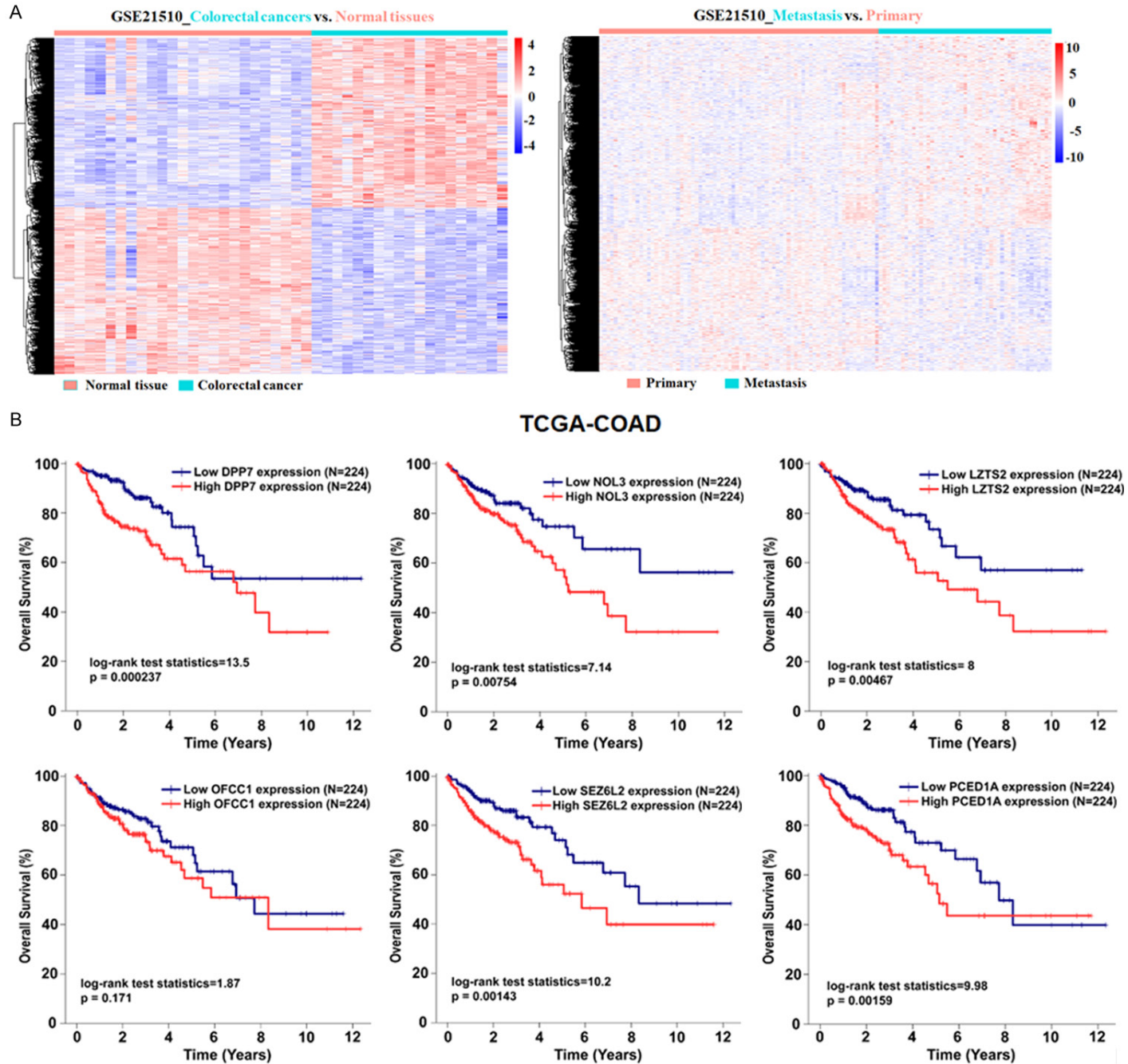# MOGS enhances colorectal cancer stemness and invasion

Supplementary Table 1. RT-qPCR primer sequences for human genes

Gene	Forward primer	Reverse primer
MOGS	CCGGGGACTCCTAAGCTCA	CCTCTTGACGAACTCAGTGGT
GAPDH	GGAGCGAGATCCCTCCAAAAT	GGCTGTTGTCATACTTCTCATGG

Supplementary Table 2. Sequences for siRNAs

siRNA	Sequences (5'-3')
si-MOGS-1	GGCAGUUCUUGAUACAGCATT
	UGCUGUAUCAAGAACUGCCTT
si-MOGS-2	GCAGUAUGUAGAUGCUCUUTT
	AAGAGCAUCUACAUACUGCTT
NC	UUCUCCGAACGUGUCACGU
	ACGUGACACGUUCGGAGAA

MOGS enhances colorectal cancer stemness and invasion

A

GSE21510_Colorectal cancers vs. Normal tissues

GSE21510_Metastasis vs. Primary

Normal tissue Colorectal cancer

Primary Metastasis

B

TCGA-COAD

Low DPP7 expression (N=224)
High DPP7 expression (N=224)

log-rank test statistics=13.5
p = 0.000237

Low NOL3 expression (N=224)
High NOL3 expression (N=224)

log-rank test statistics=7.14
p = 0.00754

Low LZTS2 expression (N=224)
High LZTS2 expression (N=224)

log-rank test statistics= 8
p = 0.00467

Low OFCC1 expression (N=224)
High OFCC1 expression (N=224)

log-rank test statistics=1.87
p = 0.171

Low SEZ6L2 expression (N=224)
High SEZ6L2 expression (N=224)

log-rank test statistics=10.2
p = 0.00143

Low PCED1A expression (N=224)
High PCED1A expression (N=224)

log-rank test statistics=9.98
p = 0.00159

2

Supplementary Figure 1. A. Left panel shows the DEGs between normal colon tissues and CRC tissues in the GSE21510 dataset. Right panel shows the DEGs between non-metastatic CRC tissues and metastatic CRC tissues in the same dataset. Red and blue denote high and low expression, respectively. B. Kaplan-Meier survival analysis of TCGA-COAD samples from the TCGA cohort.
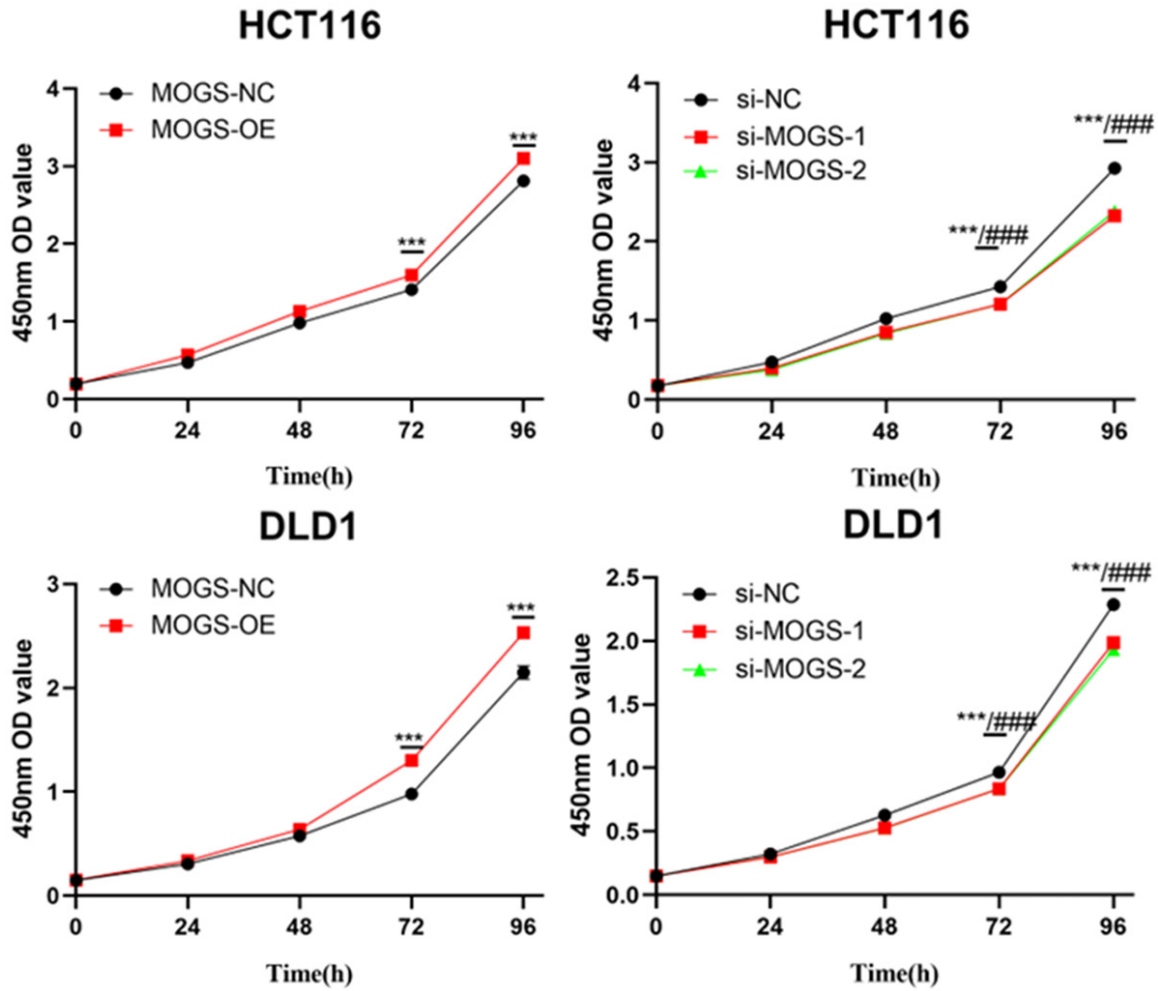
Supplementary Figure 2. CCK-8 assay for cell proliferation. Data are expressed as means ± SD. ***$P < 0.001$ vs. control. ###$P < 0.001$ si-MOGS-2 vs. control.
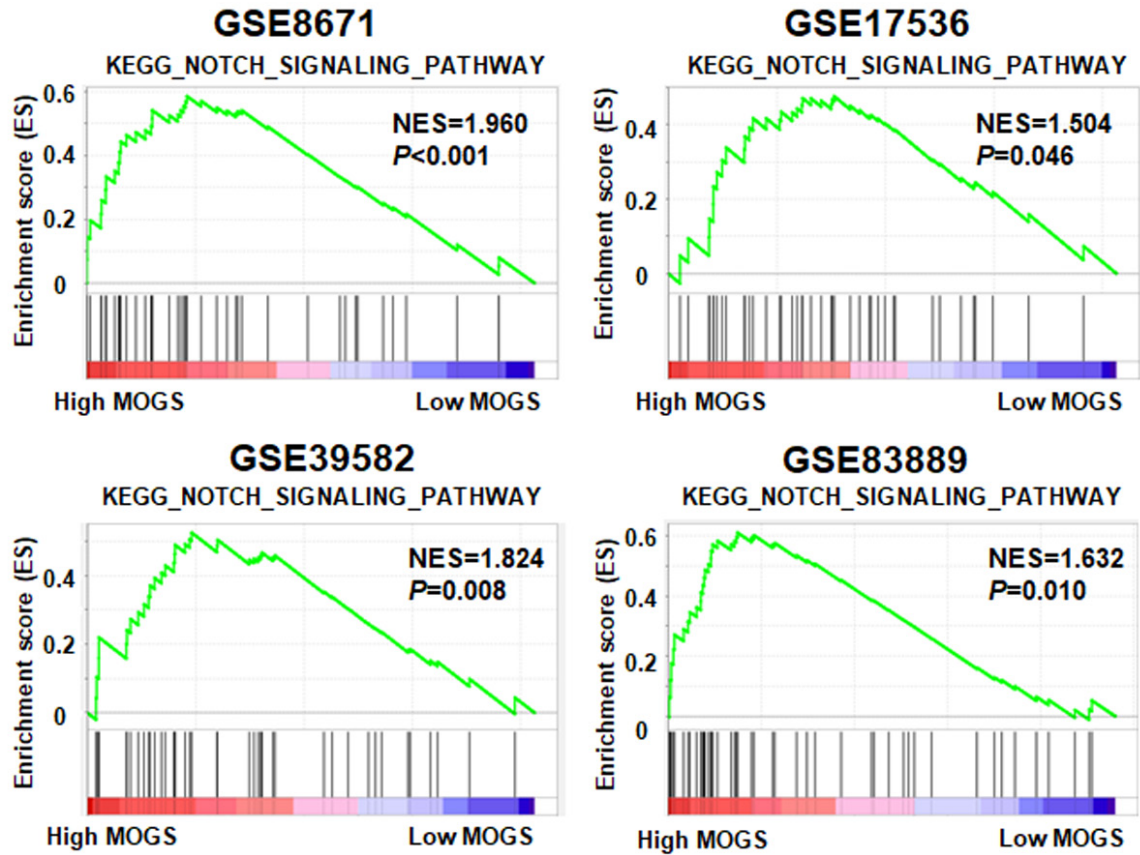
Supplementary Figure 3. Enrichment plots of NOTCH signaling pathway in GSE8671, GSE17536, GSE39582 and GSE83889 datasets.